Published in final edited form as:
Dev Biol. 2006 August 01; 296(1): 104–18. doi:10.1016/j.ydbio.2006.04.442.

Dose-dependent *Smad1*, *Smad5* and *Smad8* signaling in the early mouse embryo

Sebastian J. Arnold[#], **Silvia Maretto**[#], **Ayesha Islam**, **Elizabeth K. Bikoff**, **Elizabeth J. Robertson**[*]

Wellcome Trust Centre for Human Genetics, University of Oxford, Roosevelt Drive, Oxford, OX3 7BN, UK

[#] These authors contributed equally to this work.

Abstract

Three closely related mammalian R-Smads, namely *Smad1*, *Smad5* and *Smad8*, are activated by BMP receptors. Here we have taken a genetic approach to further dissect their possibly unique and/or shared roles during early mouse development. A *Smad8.LacZ* reporter allele was created to visualize *Smad8* expression domains. *Smad8* is initially expressed only in the visceral yolk sac (VYS) endoderm and shows a highly restricted pattern of expression in the embryo proper at later stages. In addition, *Smad8* conditional and null alleles were engineered. All alleles clearly demonstrate that adult *Smad8* homozygous mutants are viable and fertile. To elucidate gene dosage effects, we manipulated expression ratios of the three BMP R-Smads. *Smad8* homozygotes also lacking one copy of *Smad1* or *Smad5* did not exhibit overt phenotypes, and the tissue disturbances seen in *Smad1* or *Smad5* null embryos were not exacerbated in the absence of *Smad8*. However, we discovered a profound genetic interaction between *Smad1* and *Smad5*. Thus, as for *Smad1* and *Smad5* mutant embryos, *Smad1* $^{+/-}$ *:Smad5* $^{+/-}$ double heterozygotes die by E10.5 and display defects in allantois morphogenesis, cardiac looping and primordial germ cell (PGC) specification. These experiments demonstrate for the first time that *Smad1* and *Smad5* function cooperatively to govern BMP target gene expression in the early mammalian embryo.

Keywords

BMP signaling; *Smad1*; *Smad5*; *Smad8*; Early mouse development; Heart morphogenesis; Genetics

Introduction

Members of the TGFβ family of secreted growth factors regulate key processes during postimplantation mammalian development including embryonic axis patterning, organogenesis and specification of the germ line (reviewed in Chang et al., 2002; Massague et al., 2005). The ligands can be broadly divided into two groups, namely, the BMPs and activin/TGFβ/nodals in accordance with biological and structural criteria (reviewed in Massague and Chen, 2000; Massague and Wotton, 2000; Massague et al., 2000). Despite

[*]Corresponding author. Fax: +44 1865 287776. Elizabeth.Robertson@well.ox.ac.uk (E.J. Robertson).

Europe PMC Funders Author Manuscripts

considerable ligand diversity, signal transduction is controlled by only a few Smad transcription factors that are activated by cell surface receptor kinases and are highly conserved across the animal kingdom including vertebrates, insects and nematodes.

A key question is whether R-Smads have unique and/or partially overlapping functions in the early embryo. It is well known that *Smad2* and *Smad3*, acting downstream of TGFβ/activin/nodal ligands, differ in their abilities to activate or repress selected target genes (Chou et al., 2003; Labbe et al., 1998; Massague et al., 2005; Seoane et al., 2004). Mice lacking *Smad2* or *Smad3* display quite different phenotypes. Loss of *Smad2* results in embryonic lethality shortly after implantation (Heyer et al., 1999; Waldrip et al., 1998), whereas *Smad3*-deficient animals are viable and fertile (Datto et al., 1999; Zhu et al., 1998). Nonetheless, our recent experiments reveal that *Smad3* coding sequences can functionally substitute for *Smad2* during mouse development (Dunn et al., 2005). These results demonstrate that the strikingly different phenotypes are not due to divergent functional activities but rather result from the unique *Smad2* expression domain in the extra-embryonic visceral endoderm (VE), essential for inducing the anterior visceral endoderm (AVE) signaling center that patterns the early embryo (Brennan et al., 2001).

Three mammalian R-Smads, namely *Smad1*, *Smad5* and *Smad8*, are activated by BMP receptors. *Smad1* and *Smad5* have been shown to play essential roles in the early mouse embryo. *Smad5* mutants display multiple embryonic and extra-embryonic tissue defects affecting ventral closure, the heart and vascular system and allantois (Chang et al., 1999; Yang et al., 1999). *Smad1*-deficient embryos die at day 10.5 dpc due to failure to elaborate the allantois (Lechleider et al., 2001; Tremblay et al., 2001). Both *Smad1* (Hayashi et al., 2002; Tremblay et al., 2001) and *Smad5* (Chang and Matzuk, 2001) mutants display defects in PGC specification. Interestingly, the disturbances caused by mutations in the Smad genes are far less severe than the embryonic patterning defects caused by functional loss of their BMP ligands (Solloway and Robertson, 1999; Winnier et al., 1995; Zhang and Bradley, 1996) or type I Alk receptors (Gu et al., 1999; Mishina et al., 1999; Mishina et al., 1995). For example, *BMP4* mutants display gastrulation defects, with many embryos failing to form sufficient mesoderm (Winnier et al., 1995). Similarly, loss of *BMP2* function disrupts formation of both extra-embryonic and embryonic mesodermal derivatives beginning at around day 8 of development (Zhang and Bradley, 1996). The relatively late onset of *Smad1* and *Smad5* phenotypes in comparison with those observed for *BMP2* and *BMP4* mutant embryos can be explained due to functional redundancy and suggests that BMP R-Smads may share interchangeable roles as transcriptional activators of BMP target genes.

Smad1, *Smad5* and *Smad8* share striking sequence similarities, including conserved ERK/MAPK consensus phosphorylation sites in the linker region (Fig. 1A) (Aubin et al., 2004; Massague, 2003). Phylogenetic sequence comparisons indicate that *Smad8* and *Smad1/5* diverged early in vertebrate evolution (Fig. 1C). Interestingly, the linker region of both *Smad1* and *Smad5* is encoded in a single exon whereas the *Smad8* linker is encoded by two exons. In rodents, the exon encoding the C-terminal portion of the *Smad8* linker has been lost (Fig. 1B), but the short isoform retains the conserved MAPK consensus phosphorylation sites. Both *Smad8* isoforms are efficiently phosphorylated in response to activated BMP type I receptors, form complexes with *Smad4* and move to the nucleus to govern target gene

expression (Kawai et al., 2000). Such a high degree of conservation across a wide evolutionary distance strongly suggests that *Smad8* plays an important functional role in mediating BMP signaling in vertebrates.

A recent report described *Smad8* "hypomorphic" mutant mice but results were inconclusive (Hester et al., 2005). The hypomorphic allele lacking exon 3 gave no discernable phenotype, whereas an alternative targeting strategy that generates a *Smad8*–neomycin fusion protein was associated with weakly penetrant neural defects. Thus, the role played by *Smad8* in the early mammalian embryo has yet to be elucidated. Moreover, *Smad8* expression patterns remain ill defined. Here we used a genetic approach to further dissect unique and shared roles played by closely related BMP R-Smads. A *LacZ*.*Smad8* reporter allele was engineered to document highly restricted *Smad8* expression domains in the early mouse embryo. At implantation *Smad8* is exclusively expressed in the visceral endoderm, and in contrast to *Smad1* and *Smad5*, *Smad8* transcripts are undetectable in the embryo proper until E8.0. Unlike *Smad1* and *Smad5*, which are ubiquitously expressed throughout the embryo, *Smad8* shows a tightly regulated pattern of expression restricted to only a few tissue sites.

We also engineered *Smad8* conditional and null alleles. The present results clearly demonstrate that *Smad8* homozygous mutant mice are fully viable and fertile. To test the possibility that *Smad1* and/or *Smad5* compensate for *Smad8* due to functional redundancy, we used a genetic approach to manipulate gene dosage and expression ratios of the three BMP R-Smads. *Smad8* homozygotes also lacking one copy of *Smad1* or *Smad5* did not exhibit overt phenotypes. Moreover, the defects displayed by *Smad1* or *Smad5* null embryos were not exacerbated in the absence of *Smad8*. Surprisingly, however, we discovered a profound genetic interaction between *Smad1* and *Smad5*. Interestingly, the tissue disturbances in double heterozygous embryos including failure of allantois morphogenesis and cardiac defects closely resemble those seen in *Smad1* and *Smad5* homozygous mutants. These experiments demonstrate for the first time that *Smad1* and *Smad5* function cooperatively to govern BMP target gene expression in the early mammalian embryo.

Materials and methods

Generation of *Smad8* alleles

A 129/SvJ genomic library (Stratagene) was screened using a full-length *Smad8* cDNA clone as a probe to isolate *Smad8* genomic fragments. The *Smad8*. *LacZ* knock-in construct was generated by placing a *LacZ*-polyA cassette immediately upstream of the endogenous translational start site in exon 2. A 3.2-kb *Xho*I/*Kpn*I fragment was used as 3′ homology arm. A loxP flanked PGK-hygro resistance cassette was integrated between the 5′ 2.9-kb *Nhe*I/*Xho*I genomic fragment and the 3′ homology arm. The 5′ and 3′ homology arms were flanked with HSV-TK and PGK-DTA-negative selection cassettes, respectively. To generate the *Smad8* conditional construct, a loxP flanked PGK-hygromycin resistance cassette was inserted between a 2.9-kb *Nhe*I/*Xho*I subfragment as 5′ homology arm and a 7.5-kb *Xho*I/*Sal*I 3′ arm subfragment. A loxP-site and an *Nsi*I restriction site were inserted 3′ of exon 3 into the *Xba*I site. The homology regions were flanked with HSV-TK and PGK-DTA-negative selection cassettes.

Following electroporation into CCE ES cells, drug-resistant colonies were screened by Southern blot. For the *Smad8.LacZ* mutant allele, *Sac*I-digested DNAwas analyzed using a 5′ external probe. Seven of 142 clones were correctly targeted of which 2 were subjected to in vitro Cre-mediated recombination. Subclones lacking the floxed hygromycin cassette were identified via Southern blot on *Xba*I-digested samples with a 5′ internal probe. For the conditional allele, DNA from drug-resistant clones was digested with *Sac*I and screened by Southern blot analysis using a 5′ external probe. The presence of the single loxP site was confirmed with a 3′ internal probe. Eleven out of 384 clones were correctly targeted. To generate both conditional and null alleles and to confirm that the loxP sites were intact, we transiently transfected targeted clones with a pMC1Cre expression vector. The excision events were analyzed by Southern blots analyzing *Nsi*I-digested DNA with an internal probe. All possible Cre-mediated recombination events were detectable.

Cre-excised clones were injected into C57BL/6J blastocysts to generate germ line chimeras. Offspring were genotyped by Southern blot analysis and confirmatory PCR assays. Homozygous progeny from F1 intercross matings were used to establish mutant strains for each of the alleles.

Mouse strains and genotyping

The mutations were maintained on a mixed genetic background. All three *Smad8* alleles were detectable by PCR with Smad8-specific primers: *Smad8*-F3 5′-GCAGTGCCTTGGGGTTTTCA-3′, *Smad8*-R1 5′-GGGGAAACTGAGGCAAGAGA ATGG-3′ and *Smad8*-R3 5′-AAGCAGTGGGGTC-CGATTCAA-3′. PCRs were performed as follows: 94°C for 3 min followed by 35 cycles of 94°C for 15 s, 56°C for 30 s, 72°C for 30 s and 72°C extension for 7 min. Bands were separated on a 2% agarose gel resulting in 192 bp (wt), 244 bp (conditional allele), 150 bp (null allele) and 250 bp (*LacZ* allele), respectively. PCR screens for *Smad1* (Tremblay et al., 2001) and *Smad5* (Chang et al., 1999) mutant alleles have been described.

Ribonuclease protection assays

Total RNA from outbred CD1 embryos and yolk sacs was prepared using Trizol® (Invitrogen). Ribonuclease protection analysis was performed using 10 μg of total RNA according to the manufacturers' instructions (RPAIII Kit, Ambion). The *Smad1* probe corresponds to the *Nar*I–*Eco*RI fragment encompassing nucleotide positions 1100–1320 of NM008539 and spans the C-terminal portion of the linker and the N-terminal portion of the MH2 domain. The protected fragment is 220 bp. The *Smad5* probe encompassing the linker region corresponds to an *Eco*RI/*Taq*α *I* fragment spanning nucleotide positions 1128–1510 of AF063006 and protects a 383 bp fragment. The *Smad8* probe derives from exon 1 and protects the first 304 bp of the *Smad8* mRNA. Protected fragments were analyzed on 5% PAGE gels, exposed to film and quantified by Biorad Personal Molecular Imager FX with BioRad GE Heathcare Quantity One® software.

In situ hybridization, X-Gal staining and histology

Whole-mount in situ hybridization analysis was performed according to standard procedures (Hogan et al., 1994). Probes specific for *eHand* (Cserjesi et al., 1995), *FGF8* (Crossley and

Martin, 1995), *MLC2V* (Lyons et al., 1995b), *Nodal* (Conlon et al., 1994), *Smad1* (Waldrip et al., 1998), *Smad5* (Meersseman et al., 1997) and *Twist* (Fuchtbauer, 1995) have been described. The *Smad8* probe comprised the full-length cDNA. Up to E10.5 X-Gal staining was performed on whole embryos as described (Hogan et al., 1994). Older stage embryos were fixed in 4% PFA/PBS for 2 h, embedded in 3% agarose/PBS, sectioned at 300 μm on a Leica VT 1000S vibratome and stained for X-Gal activity. For histology, embryonic tissues were postfixed in 4% PFA, dehydrated through an ethanol series and embedded in paraffin before sectioning at 8 μm. Hematoxylin and eosin staining was performed according to standard procedures.

Visualization of PGCs

Primordial germ cells were visualized in E8.5 and 9.5 embryos by alkaline phosphatase staining as described (Ginsburg et al., 1990; Lawson et al., 1999). Embryos were dissected in PBS, fixed for 2 h at 4°C in 4% PFA, washed 3 times in PBS, and either maintained intact as whole embryos (E8.5) or further dissected (E9.5). In this case, embryos were split into an anterior and posterior portion at the forelimb level, and posterior portions were split longitudinally along the dorsal aorta to remove the somites, unsegmented paraxial mesoderm and neural tube. Fragments were then treated with 70% ethanol for 1 h at 4°C, washed three times with distilled water and stained with α-naphtyl phosphate/fast red (Sigma F4523) for 45 min at room temperature. Stained embryos or dissected fragments were washed in water and transferred to 75% glycerol to clear. Specimens were flattened on a slide under a coverslip prior to photography.

Results

Highly restricted *Smad8* expression domains at early stages of mouse development

We previously used radioactive in situ hybridization techniques to study *Smad1*, *Smad5* and *Smad8* expression at early stages, but it was difficult to visualize discrete signals in E6.5, 7.5 and 8.5 sagittal sections (Tremblay et al., 2001). In particular, *Smad8* gave an extremely weak hybridization signal just barely detectable above background. To compare expression patterns, we performed whole mount in situ hybridization on intact postimplantation embryos (Figs. 2A–F). As expected, we observed that *Smad1* and *Smad5* are broadly expressed throughout the extra-embryonic and embryonic regions (Chang et al., 1999; Tremblay et al., 2001). In contrast, *Smad8* is initially confined to the VYS endoderm at E7.5, later by E9.5 expression within the embryo is localized to the developing heart, including the heart tube and surrounding mesenchyme and the tail bud (Figs. 2C and F).

To further examine BMP R-Smad expression ratios, we performed RNase protection assays (RPA) (Figs. 2G and H). Consistent with results above, we found *Smad1* and *Smad5* mRNAs were strongly co-expressed from E7.5 onwards. We consistently detect increased levels of *Smad1* in the yolk sac, whereas *Smad5* is slightly more abundant in the embryo proper. In contrast, *Smad8* transcripts are mainly detectable in the VYS and only marginally in the embryo proper (Fig. 2H). In comparison with *Smad1* and *Smad5*, we detect considerably less *Smad8* expression in the VYS. These results suggest that *Smad1* and *Smad5* function as the predominant transcriptional regulators of target gene expression

throughout development whereas *Smad8* probably serves to modulate BMP signals in selected cell types.

Generation of *Smad8* null, conditional and LacZ reporter alleles

To more precisely delineate *Smad8* expression domains, we introduced an in-frame *LacZ* cassette into exon 2, the first coding exon of the locus (Fig. 3A). We also decided to generate both a null and conditional allele by flanking exons 2 and 3 with loxP sequences (Fig. 3C). Cre-mediated recombination is predicted to eliminate the initial 180 residues comprising the MH1 domain and most of the linker region.

Embryos carrying the *Smad8.LacZ* reporter allele were recovered from early postimplantation stages onwards and stained for β-galactosidase activity. As expected, *LacZ* expression is first detected in the VE overlying the extra-embryonic ectoderm at E6.0 and is maintained in the VE of the yolk sac throughout gestation (Figs. 4A, B, B′ and data not shown). *LacZ* activity is undetectable within the embryo proper until early somite stages, when low levels of expression become apparent in the region of the heart and the tail bud and allantois (Fig. 4C). By E9.5, *LacZ* staining is regionalized within the heart tube being confined to the myocardial layer of the outflow tract but the forming ventricles lack *Smad8.LacZ* expression (Figs. 4D, D′ and D″). We also detect *Smad8.LacZ* expression in the inner (neural) layer of the developing optic vesicle (Figs. 4E, E′ and G).

At later stages, *Smad8.LacZ* staining was detectable in all sites of forming cartilage associated with the axial, appendicular and cranial skeleton (Figs. 4G and 5A–C). Heart expression resolves to the tissue separating the atria from the ventricles (Figs. 5D and E). In the kidney, *Smad8.LacZ* expression is detectable in the epithelium of Bowman's capsule, proximal tubules and collecting ducts and in cells comprising the juxtaglomerular apparatus (Fig. 5G). In the lung, *LacZ* staining is mainly seen in the endodermal component of the bronchioles (Fig. 5I). *Smad8* is strongly expressed in the outer muscular layer and in the outer endodermal layer of the gut villi along the entire length of the gut tube (Figs. 5A, C and H). Within the developing CNS, we detect a very restricted expression pattern for *Smad8*. For example, focal expression is seen in the choroid plexus and groups of interneurons in the spinal cord (Figs. 5B, C and F). The tightly regulated *Smad8.LacZ* expression pattern described here strengthens the idea that *Smad8* regulates BMP signaling in a highly restricted cell context-dependent fashion.

Smad8 mutant mice develop normally and are viable and fertile

Recent experiments suggest that *Smad8* may play a role in the developing CNS (Hester et al., 2005). A small proportion of homozygous embryos expressing a *Smad8*–neomycin fusion protein display increased cellularity of the hindbrain. However, animals carrying a hypomorphic *Smad8* allele lacking exon3 sequences develop normally (Hester et al., 2005). To clarify these contradictory conclusions and evaluate possible *Smad8* requirements in vivo, our *Smad8* $^{+/-}$ heterozygotes were intercrossed. As shown in Table 1A, *Smad8* null homozygotes were recovered at Mendelian frequencies. *Smad8* mutants of both sexes were overtly indistinguishable from littermates and proved to have normal fertility and fecundity in breeding experiments. Moreover, homozygotes carrying the *Smad8.LacZ* reporter allele in

which the *LacZ* cassette inserted into exon 2 disrupts the endogenous coding sequence were also perfectly healthy. We conclude that *Smad8* plays a nonessential role and that the abnormalities previously reported in *Smad8* mutants (Hester et al., 2005) most probably arise due to dominant effects of the neomycin fusion protein.

We also intercrossed *Smad8* mutants with *Smad1* (Tremblay et al., 2001) and *Smad5* (Chang et al., 1999) null alleles to test for possible functional redundancy (Tables 1B and C). Reducing *Smad1* or *Smad5* expression levels in the context of the *Smad8* mutation fails to cause any noticeable disturbances. Thus, *Smad8* $^{-/-}$ *:Smad1* $^{+/-}$ and *Smad8* $^{-/-}$ *: Smad5* $^{+/-}$ animals were recovered at the predicted Mendelian ratios. Next, we intercrossed *Smad8* $^{-/-}$ *:Smad1* $^{+/-}$ or *Smad8* $^{-/-}$ *: Smad5* $^{+/-}$ animals. At E10.5, *Smad8* $^{-/-}$ *:Smad1* $^{-/-}$ and *Smad8* $^{-/-}$ *:Smad5* $^{-/-}$ double homozygous embryos display the same phenotypes as those described previously for *Smad1* or *Smad5* null mutant embryos (data not shown). Given that *Smad8* is co-expressed with *Smad1* and *Smad5* only in the VYS of the early embryo (Fig. 2), particular care was taken to examine the morphology of the visceral yolk sac. However, there was no evidence for exacerbated phenotypes associated with the loss of *Smad8* expression.

Smad1 $^{+/-}$:*Smad5* $^{+/-}$ double heterozygous embryos die by E10.5

To further evaluate dose-dependent BMP R-Smad signaling thresholds, we attempted to reduce both *Smad1* and *Smad5* expression levels. Intercrosses between *Smad8* $^{-/-}$ *:Smad1* $^{+/-}$ and *Smad8* $^{-/-}$:*Smad5* $^{+/-}$ animals were set up to generate F1 *Smad8* $^{-/-}$:*Smad1* $^{+/-}$:*Smad5* $^{+/-}$ progeny. From a panel (>100) of live born animals, none proved to be double heterozygotes (Table 1D). Lowering the dose of both *Smad1* and *Smad5* clearly results in embryonic lethality. We were curious to learn whether the phenotype depends on the loss of *Smad8* function. To test this possibility, we intercrossed *Smad1* $^{+/-}$:*Smad8* $^{+/+}$ and *Smad5* $^{+/-}$:*Smad8* $^{+/+}$ animals. Also in this case no live born double heterozygous offspring were recovered (data not shown). A panel of E13.5 embryos (n = 42) from intercross matings showed that the *Smad1* $^{+/-}$:*Smad5* $^{+/-}$ double hetero-zygotes were lost by this stage of development although a number of resorption sites were noted. Although not tested formally because the phenotypes of *Smad8* $^{-/-}$:*Smad5* $^{+/-}$: *Smad1* $^{+/-}$ were not examined, the *Smad1/5* genetic interaction is independent of *Smad8* expression because of the very limited domain of *Smad8* expression in the early embryo (Fig. 2).

Smad1 $^{+/-}$:*Smad5* $^{+/-}$ double heterozygotes were readily identifiable at E10.5 and E11.5. As for *Smad1* and *Smad5* mutants, we also observe a diverse spectrum of tissue abnormalities (Fig. 6). The various classes of double heterozygous embryos, as summarized in Table 2, encompass the entire range of disturbances described for *Smad1*- and *Smad5*-deficient embryos. The most severely affected embryos (approximately 33%), as for *Smad5* null embryos (Chang et al., 1999), were poorly patterned along the anterior–posterior axis and failed to initiate the process of embryonic turning (Figs. 6E and G). On the other hand, many embryos were overtly normal except that the allantois remained as a dense mass of tissue (Fig. 6C), as described for *Smad1* null mutants (Lechleider et al., 2001; Tremblay et al., 2001). Interestingly, at E7.5 a proportion of the double heterozygous mutants also displayed a pronounced ruffling of the VYS endoderm (Fig. 6A) characteristic of *Smad1* but not

Smad5 mutants. Furthermore, we observed some mutant embryos in which the allantois tissue was fused across the amnion, a phenotype that is distinctive of Smad5-deficient embryos (Chang et al., 1999). Pronounced heart looping defects were also evident in a high proportion of embryos.

To further characterize the tissue defects, we used a panel of molecular markers. The bHLH gene *Twist* was used as a pan marker of mesenchyme. As shown in Fig. 6G, in the most severely affected mutants, mesoderm was underrepresented. The second and third branchial arches were absent or severely compromised in their development. Similar defects have been described in *Smad5* mutants (Chang et al., 1999) and *BMP5/7* double null embryos (Solloway and Robertson, 1999). As seen in *BMP5/7* mutants, we observed in a proportion of double *Smad1* $^{+/-}$:*Smad5* $^{+/-}$ heterozygous embryos that the somites were often misaligned and fragmented (Fig. 6H). *Fgf8* expression normally delineates the anterior-most forebrain, the isthmus separating the mid- and hindbrain and the branchial arches. *Fgf8* expression domains reveal a spectrum of anterior defects (Fig. 6J). As for *Smad5* mutant embryos, in the majority of the more severely affected embryos (Chang et al., 1999), the most rostral regions of the CNS were absent, whereas in other cases, the tissue was correctly specified, but the cranial folds had failed to fuse (Fig. 7B).

Smad1 $^{+/-}$:*Smad5* $^{+/-}$ double heterozygous embryos display heart looping and laterality defects

Heart morphogenesis and patterning is severely disturbed in *Smad5* mutant embryos (Chang et al., 2000). We also found here that *Smad1* $^{+/-}$:*Smad5* $^{+/-}$ embryos consistently display defects in early heart development. Fusion of the bilateral heart primordia to form the heart tube always occurs, but subsequent morphogenesis is disturbed. As shown in Fig. 7, we observe a range of phenotypes including inversion in the direction of looping, stalled looping with the heart tube remaining linear along the ventral midline, and normal rightward looping. Sections of affected hearts showed that the endocardium had formed normally (data not shown). However, even in cases where the direction of heart looping was correct, overt patterning of the forming heart chambers was severely abnormal. In situ hybridization with *eHand*, a basic helix–loop–helix gene normally expressed primarily on the outer curvature of the developing left ventricle (Biben and Harvey, 1997), revealed major disturbances in chamber specification (Figs. 7E–H). In the majority of *Smad1* $^{+/-}$:*Smad5* $^{+/-}$ double heterozygotes, the *eHand* expression domain expands to mark myocardial cells situated more cranially and becomes symmetrically expressed (Fig. 7F). Looping morphogenesis defects may therefore be a secondary consequence of failure to appropriately pattern the A–P axis of the heart tube.

Heart looping defects in *Smad5*-deficient embryos have been attributed in part to inappropriate establishment of the L/R axis (Chang et al., 2000). To investigate establishment of the L/R body axis in *Smad1* $^{+/-}$:*Smad5* $^{+/-}$ double heterozygotes, we examined expression of the TGFβ. ligand *Nodal. Nodal* is the first gene to become asymmetrically activated in the lateral plate, where it initiates a signaling cascade that governs induction of key target genes namely *lefty1*, *lefty2* and the transcription factor *Pitx2* (reviewed in Schier, 2003). At early somite stages, the double mutant embryos all showed

appropriate *Nodal* expression in the node, but staining patterns in the lateral plate mesoderm were disturbed. Leftsided, bilateral and right-sided expression as well as complete failure to activate *Nodal* expression were observed (Figs. 7I–L). Thus, we conclude that *Smad1* $^{+/-}$:*Smad5* $^{+/-}$ double heterozygous embryos are compromised in their ability to correctly activate the L/R pathway in the lateral plate mesoderm.

Severely impaired PGC specification in *Smad1* $^{+/-}$:*Smad5* $^{+/-}$ double heterozygotes

BMP signaling from the extra-embryonic ectoderm is essential for inducing formation of PGCs in the adjacent proximal epiblast prior to gastrulation (reviewed in McLaren, 2003). The pathway for germ cell specification is known to be highly dose dependent. Thus, loss of *BMP4* disrupts PGC specification and fewer germ cells are specified in *BMP4* heterozygotes (Lawson et al., 1999; Ying and Zhao, 2001). *Smad1* (Hayashi et al., 2002; Tremblay et al., 2001), *Smad5* (Chang and Matzuk, 2001) and *Smad4* (Chu et al., 2004) activities are required for PGC specification. We wondered if decreased *Smad1*/*5* expression levels might also cause PGC defects in double heterozygous embryos. PGCs can be readily recognized from E7.5 onwards due to their high levels of endogenous alkaline phosphatase (AP) activity. AP-positive PGCs are first seen at the base of the allantois, then enter the dorsal hindgut as gastrulation proceeds. To examine PGC specification, we examined PGC numbers in 10–15 and 20–25 somite stage (early forelimb bud) double heterozygous embryos in which ventral closure and gut formation had proceeded normally. By 10–15 somite stages, approximately 80–100 PGCs are detectable in the dorsal wall of the gut tube of wild-type embryos (Figs. 8A and A′). In contrast, age-matched double heterozygotes contain markedly reduced PGC numbers (Figs. 8B and B′). By 20–25 somites, between 200 and 300 AP-positive germ cells are normally present in the dorsal hindgut (Fig. 8C). The majority of double heterozygotes entirely lack germ cells, whereas in the remainder (<40%) we observe ~ 10-fold fewer AP-positive cells (Fig. 8E). These results demonstrate that dose-dependent *Smad1/5* signals regulate allocation of the germ cell founder population at very earliest stages.

Discussion

The wide range of biological responses elicited by BMPs, the largest subfamily of TGFβ secreted growth factors, converge on three closely related downstream effectors, *Smad1*, *Smad5* and *Smad8*. *Smad1* and *Smad5* show the highest degree of sequence conservation whereas *Smad8* is more structurally divergent (Figs. 1A and C). *Smad8* is conserved in the genomes of all vertebrates. In contrast to *Smad1* and *Smad5*, both strongly expressed throughout the embryo, we demonstrate here that *Smad8* is initially confined to the visceral endoderm. From E9.5 *Smad8* shows a tightly regulated pattern of expression within the embryo localized to the early heart, eye, gut endoderm, subsets of cells in the lung, kidney and throughout the developing skeleton. These results suggest that *Smad8* expression at discrete tissue sites may act to modulate BMP signaling in selected cell types.

In the developing eye, the lens-specific promoter of the *Foxe3* transcription factor is specifically regulated via a *Sip-1*/*Smad8* complex (Yoshimoto et al., 2005). Nonetheless, we observe that lens morphogenesis proceeds normally in the absence of *Smad8*. Intriguingly,

the *Smad8* expression pattern described here closely resembles that of an Id SBE-LacZ transgene reporter that specifically detects sites of active BMP signaling (Monteiro et al., 2004). Particularly robust reporter activity was seen in the dorsal optic vesicle and the heart. We speculate that *Smad8* transcription could potentially be a BMP target. This is not without precedence because expression of the inhibitory Smads, *Smad6* and *Smad7*, is up-regulated by BMP/TGFβ. signaling to provide a negative feedback circuit (Imamura et al., 1997; Nakao et al., 1997). An attractive possibility is that *Smad8* functions synergistically to up-regulate *Smad1*/*5* activities.

In humans, a recent report described consistent epigenetic silencing of *Smad8* via DNA hypermethylation in multiple cancer types, including 30% of breast and colon cancer samples surveyed (Cheng et al., 2004). These observations suggest that *Smad8* may serve as a negative regulator of cell growth particularly in the mammary gland and gut endoderm. The present experiments clearly demonstrate that *Smad8* mutant mice develop normally and are viable and fertile. Further experiments exploiting the available *Smad1* (Tremblay et al., 2001), *Smad5* (Umans et al., 2003) and *Smad8* conditional alleles will be required to describe possible *Smad8* functions regulating organogenesis and homeostatic processes.

In zebrafish, both *Smad1* and *Smad5* are involved in specification of the dorsal–ventral axis. Interestingly, *Smad5* is expressed both maternally and zygotically and is required downstream of *BMP2b* signaling to induce *Smad1* ventrally (Dick et al., 1999; Suzuki et al., 1997). The dorsalized phenotype of *BMP2b* mutant embryos can be rescued by exogenous *Smad1* but not *Smad5*. Thus, previous studies point to unique functions for the Zebrafish *Smad1* and *Smad5* homologs. On the other hand, in mouse both *Smad1* and *Smad5* mutant embryos display a wide spectrum of partially overlapping tissue defects (Chang et al., 1999, 2000; Chang and Matzuk, 2001; Lechleider et al., 2001; Tremblay et al., 2001; Yang et al., 1999). Overall, the *Smad5* phenotype is more severe because only a small proportion of embryos achieve turning (Chang et al., 1999; Table 2). *Smad1*-deficient embryos fail to establish a connection with the placenta due to failure of allantois growth but otherwise develop more normally. These distinctive phenotypes could potentially reflect subtle differences in the relative expression ratios in distinct cell lineages of the embryo. Thus, our RPA experiments consistently demonstrate increased *Smad1* expression in the early VYS, perhaps accounting for ruffled yolk sacs in the mutants (Tremblay et al., 2001). In contrast *Smad5* mRNA is more strongly expressed in the embryo proper.

The present report documents a profound *Smad1*/*5* genetic interaction. The striking phenotypic similarity shared between *Smad1* $^{+/-}$:*Smad5* $^{+/-}$ double heterozygous embryos and those lacking *Smad1* or *Smad5* strongly suggests that signaling functions mediated by *Smad1* and *Smad5* are equivalent. The developmental defects caused by progressive loss of *Smad1/5* signals are summarized in Table 2. As for *BMP4* phenotypes (Lawson et al., 1999), genetic background effects may possibly contribute to this variability because both *Smad1* and *Smad5* mutations have been maintained on an outbred background. However, variable penetrance of the *Smad1* phenotype has also been documented in 129/Sv inbred mice (Tremblay et al., 2001). Early embryonic and extra-embryonic mesodermal cell lineages are exposed to a continuously changing signaling environment and are required to accurately interpret ligand concentrations. The present experiments demonstrate that combinatorial

functional activities of *Smad1* and *Smad5* during mesoderm formation and patterning must be maintained above a critical threshold level roughly equivalent to three copies of *Smad1/5* to promote rapid growth and cell migration.

Consistent with this way of thinking, BMP ligands are expressed in partially overlapping patterns (Dudley and Robertson, 1997; Lyons et al., 1995a; Solloway and Robertson, 1999) and genetic studies strongly argue that closely related BMP family members are functionally redundant in vivo. For example, *BMP5* and *BMP6* are co-expressed from early postimplantation stages onwards (Solloway and Robertson, 1999) and functional loss of either alone fails to perturb embryonic development (Kingsley et al., 1992; Solloway et al., 1998). *BMP7* widely expressed throughout the embryo is essential only to promote eye and kidney development (Dudley and Robertson, 1997; Luo et al., 1995), whereas other tissues such as the notochord, surface ectoderm and heart that also express *BMP5* and/or *BMP6* develop normally. *BMP5/7* and *BMP6/7* double mutants show profound early phenotypes and die by mid-gestation (Kim et al., 2001; Solloway and Robertson, 1999). Interestingly, both *BMP4* or *BMP6*, structurally divergent ligands, can functionally substitute for loss of *BMP7* and rescue kidney development (Oxburgh et al., 2005). Thus, considerable evidence strongly argues that BMP signals act combinatorially.

Activin signaling thresholds in *Xenopus* result from varying degrees of receptor occupancy at the cell surface, and dose-dependent *Smad2* phosphorylation in turn modulates target gene expression (Dyson and Gurdon, 1998). Similarly, we have previously shown that progressively lowering dose-dependent *Smad2* and *Smad3* signals in the mouse embryo results in discrete phenotypic thresholds during gastrulation (Dunn et al., 2005; Vincent et al., 2003). *Smad3*-deficient embryos are viable, but removal of one copy of *Smad2* results in failure to specify axial mesendoderm. Progressive loss of *Smad3* in the context of a *Smad2*-deficient epiblast eventually disrupts node and axial mesoderm formation. Further reduction of *Smad2/3* signals compromises paraxial and lateral mesoderm formation. These genetic manipulations demonstrate a strict dose response relationship between *Smad2/3* expression levels and cell type specification (Dunn et al., 2005; Vincent et al., 2003).

The present experiments demonstrate for the first time that combinatorial activities of *Smad1* and *Smad5* regulate mesoderm patterning in the mouse embryo. As for *Smad1* and *Smad5* mutants, $Smad1^{+/-}$:$Smad5^{+/-}$ double heterozygous embryos display L/R and heart patterning defects. $Smad1^{+/-}$:$Smad5^{+/-}$ double heterozygotes also show defective allantois morphogenesis and PCG specification, cell types known to require maximal BMP signaling. PCG specification is abolished or greatly reduced in *Smad1/5* double heterozygotes, suggesting that R-Smads act combinatorially downstream of *BMP4* to control this process. It would of course be interesting to test whether *Smad1/5* double null embryos display more severe, earlier onset tissue abnormalities. Unfortunately, this possibility cannot be tested due to the inability to generate $Smad1^{+/-}$: $Smad5^{+/-}$ double heterozygous animals.

Previous work has shown that the three mammalian BMP R-Smads, *Smad1*, *Smad5* and *Smad8* signal downstream of activated *Alk3* and *Alk6* receptors (Aoki et al., 2001). On the other hand, considerable evidence suggests that *Smad1*, *Smad5* and *Smad8* also exhibit discrete activities in selected cell types. For example, *Smad1* and *Smad5* but not *Smad8* are

phosphorylated in response to stimulation of C2C12 cells by exogenous *BMP6* (Ebisawa et al., 1999). This observation may in part result due to the inability of *Alk2*, the preferred receptor for *BMP6* (Aoki et al., 2001), to efficiently phosphorylate *Smad8*. Relatively little is known about how *Smad1*, *Smad5* and *Smad8* associate with *Smad4* and enter the nucleus. Additional factors may also govern phosphorylation of *Smad1*, *Smad5* and *Smad8* by BMP receptors. The present experiments strongly argue that *Smad1* and *Smad5* share equivalent functional activities in the early embryo. Considering that BMPs elicit a wide range of biological responses in diverse cell types it will be interesting to learn whether BMP R-Smads may have unique functions controlling cell proliferation, differentiation and tissue homeostasis in the context of the adult organism.

Acknowledgments

We thank Marty Matzuk for generously providing *Smad5* mutants, Yinghui Zhou for vector construction, Dorian Anderson for RPA probes and WISH data, Jennifer Taylor for help with sequence alignments, Clive Joyner for help with histology, Carol Paterson and Emily Lejsek for animal husbandry and genotyping and Ray Dunn for advice on germ cell staining. SJA is recipient of a Feodor Lynen-Fellowship from the Alexander von Humboldt-Foundation. The work was supported by the Wellcome Trust.

References

Aoki H, Fujii M, Imamura T, Yagi K, Takehara K, Kato M, Miyazono K. Synergistic effects of different bone morphogenetic protein type I receptors on alkaline phosphatase induction. J Cell Sci. 2001; 114:1483–1489. [PubMed: 11282024]

Aubin J, Davy A, Soriano P. In vivo convergence of BMP and MAPK signaling pathways: impact of differential *Smad1* phosphorylation on development and homeostasis. Genes Dev. 2004; 18:1482–1494. [PubMed: 15198985]

Biben C, Harvey RP. Homeodomain factor Nkx2-5 controls left/right asymmetric expression of bHLH gene eHand during murine heart development. Genes Dev. 1997; 11:1357–1369. [PubMed: 9192865]

Brennan J, Lu CC, Norris DP, Rodriguez TA, Beddington RS, Robertson EJ. Nodal signalling in the epiblast patterns the early mouse embryo. Nature. 2001; 411:965–969. [PubMed: 11418863]

Chang H, Matzuk MM. *Smad5* is required for mouse primordial germ cell development. Mech Dev. 2001; 104:61–67. [PubMed: 11404080]

Chang H, Huylebroeck D, Verschueren K, Guo Q, Matzuk MM, Zwijsen A. *Smad5* knockout mice die at mid-gestation due to multiple embryonic and extraembryonic defects. Development. 1999; 126:1631–1642. [PubMed: 10079226]

Chang H, Zwijsen A, Vogel H, Huylebroeck D, Matzuk MM. *Smad5* is essential for left–right asymmetry in mice. Dev Biol. 2000; 219:71–78. [PubMed: 10677256]

Chang H, Brown CW, Matzuk MM. Genetic analysis of the mammalian transforming growth factor-beta superfamily. Endocr Rev. 2002; 23:787–823. [PubMed: 12466190]

Cheng KH, Ponte JF, Thiagalingam S. Elucidation of epigenetic inactivation of SMAD8 in cancer using targeted expressed gene display. Cancer Res. 2004; 64:1639–1646. [PubMed: 14996722]

Chou WC, Prokova V, Shiraishi K, Valcourt U, Moustakas A, Hadzopoulou-Cladaras M, Zannis VI, Kardassis D. Mechanism of a transcriptional cross talk between transforming growth factor-betaregulated Smad3 and Smad4 proteins and orphan nuclear receptor hepatocyte nuclear factor-4. Mol Biol Cell. 2003; 14:1279–1294. [PubMed: 12631740]

Chu GC, Dunn NR, Anderson DC, Oxburgh L, Robertson EJ. Differential requirements for *Smad4* in TGFbeta-dependent patterning of the early mouse embryo. Development. 2004; 131:3501–3512. [PubMed: 15215210]

Conlon FL, Lyons KM, Takaesu N, Barth KS, Kispert A, Herrmann B, Robertson EJ. A primary requirement for nodal in the formation and maintenance of the primitive streak in the mouse. Development. 1994; 120:1918–1928.

Europe PMC Funders Author Manuscripts

Crossley PH, Martin GR. The mouse Fgf8 gene encodes a family of polypeptides and is expressed in regions that direct outgrowth and patterning in the developing embryo. Development. 1995; 121:439–451. [PubMed: 7768185]

Cserjesi P, Brown D, Lyons GE, Olson EN. Expression of the novel basic helix–loop–helix gene eHAND in neural crest derivatives and extraembryonic membranes during mouse development. Dev Biol. 1995; 170:664–678. [PubMed: 7649392]

Datto MB, Frederick JP, Pan L, Borton AJ, Zhuang Y, Wang XF. Targeted disruption of *Smad3* reveals an essential role in transforming growth factor beta-mediated signal transduction. Mol Cell Biol. 1999; 19:2495–2504. [PubMed: 10082515]

Dick A, Meier A, Hammerschmidt M. *Smad1* and *Smad5* have distinct roles during dorsoventral patterning of the zebrafish embryo. Dev Dyn. 1999; 216:285–298. [PubMed: 10590480]

Dudley AT, Robertson EJ. Overlapping expression domains of bone morphogenetic protein family members potentially account for limited tissue defects in BMP7 deficient embryos. Dev Dyn. 1997; 208:349–362. [PubMed: 9056639]

Dunn NR, Koonce CH, Anderson DC, Islam A, Bikoff EK, Robertson EJ. Mice exclusively expressing the short isoform of *Smad2* develop normally and are viable and fertile. Genes Dev. 2005; 19:152–163. [PubMed: 15630024]

Dyson S, Gurdon JB. The interpretation of position in a morphogen gradient as revealed by occupancy of activin receptors. Cell. 1998; 93:557–568. [PubMed: 9604931]

Ebisawa T, Tada K, Kitajima I, Tojo K, Sampath TK, Kawabata M, Miyazono K, Imamura T. Characterization of bone morphogenetic protein-6 signaling pathways in osteoblast differentiation. J Cell Sci. 1999; 112(Pt. 20):3519–3527. [PubMed: 10504300]

Fuchtbauer EM. Expression of M-twist during postimplantation development of the mouse. Dev Dyn. 1995; 204:316–322. [PubMed: 8573722]

Ginsburg M, Snow MH, McLaren A. Primordial germ cells in the mouse embryo during gastrulation. Development. 1990; 110:521–528. [PubMed: 2133553]

Gu Z, Reynolds EM, Song J, Lei H, Feijen A, Yu L, He W, MacLaughlin DT, van den Eijnden-van Raaij J, Donahoe PK, Li E. The type I serine/threonine kinase receptor ActRIA (ALK2) is required for gastrulation of the mouse embryo. Development. 1999; 126:2551–2561. [PubMed: 10226013]

Hayashi K, Kobayashi T, Umino T, Goitsuka R, Matsui Y, Kitamura D. *Smad1* signaling is critical for initial commitment of germ cell lineage from mouse epiblast. Mech Dev. 2002; 118:99–109. [PubMed: 12351174]

Hester M, Thompson JC, Mills J, Liu Y, El-Hodiri HM, Weinstein M. *Smad1* and *Smad8* function similarly in mammalian central nervous system development. Mol Cell Biol. 2005; 25:4683–4692. [PubMed: 15899870]

Heyer J, Escalante-Alcalde D, Lia M, Boettinger E, Edelmann W, Stewart CL, Kucherlapati R. Postgastrulation *Smad2*-deficient embryos show defects in embryo turning and anterior morphogenesis. Proc Natl Acad Sci U S A. 1999; 96:12595–12600. [PubMed: 10535967]

Hogan, B, Beddington, R, Costantini, F, Lacy, E. Manipulating the Mouse Embryo, A Laboratory Manual. Cold Spring Harbor Laboratory Press; Cold Spring Harbor, NY: 1994.

Imamura T, Takase M, Nishihara A, Oeda E, Hanai J, Kawabata M, Miyazono K. *Smad6* inhibits signalling by the TGF-beta superfamily. Nature. 1997; 389:622–626. [PubMed: 9335505]

Kawai S, Faucheu C, Gallea S, Spinella-Jaegle S, Atfi A, Baron R, Roman SR. Mouse *Smad8* phosphorylation downstream of BMP receptors ALK-2, ALK-3, and ALK-6 induces its association with *Smad4* and transcriptional activity. Biochem Biophys Res Commun. 2000; 271:682–687. [PubMed: 10814522]

Kim RY, Robertson EJ, Solloway MJ. Bmp6 and Bmp7 are required for cushion formation and septation in the developing mouse heart. Dev Biol. 2001; 235:449–466. [PubMed: 11437450]

Kingsley DM, Bland AE, Grubber JM, Marker PC, Russell LB, Copeland NG, Jenkins NA. The mouse short ear skeletal morphogenesis locus is associated with defects in a bone morphogenetic member of the TGF beta superfamily. Cell. 1992; 71:399–410. [PubMed: 1339316]

Labbe E, Silvestri C, Hoodless PA, Wrana JL, Attisano L. *Smad2* and *Smad3* positively and negatively regulate TGF beta-dependent transcription through the forkhead DNA-binding protein FAST2. Mol Cell. 1998; 2:109–120. [PubMed: 9702197]

Lawson KA, Dunn NR, Roelen BA, Zeinstra LM, Davis AM, Wright CV, Korving JP, Hogan BL. Bmp4 is required for the generation of primordial germ cells in the mouse embryo. Genes Dev. 1999; 13:424–436. [PubMed: 10049358]

Lechleider RJ, Ryan JL, Garrett L, Eng C, Deng C, Wynshaw-Boris A, Roberts AB. Targeted mutagenesis of *Smad1* reveals an essential role in chorioallantoic fusion. Dev Biol. 2001; 240:157–167. [PubMed: 11784053]

Luo G, Hofmann C, Bronckers AL, Sohocki M, Bradley A, Karsenty G. BMP-7 is an inducer of nephrogenesis, and is also required for eye development and skeletal patterning. Genes Dev. 1995; 9:2808–2820. [PubMed: 7590255]

Lyons KM, Hogan BL, Robertson EJ. Colocalization of BMP 7 and BMP 2 RNAs suggests that these factors cooperatively mediate tissue interactions during murine development. Mech Dev. 1995a; 50:71–83. [PubMed: 7605753]

Lyons I, Parsons LM, Hartley L, Li R, Andrews JE, Robb L, Harvey RP. Myogenic and morphogenetic defects in the heart tubes of murine embryos lacking the homeo box gene Nkx2-5. Genes Dev. 1995b; 9:1654–1666. [PubMed: 7628699]

Massague J. Integration of Smad and MAPK pathways: a link and a linker revisited. Genes Dev. 2003; 17:2993–2997. [PubMed: 14701870]

Massague J, Chen YG. Controlling TGF-beta signaling. Genes Dev. 2000; 14:627–644. [PubMed: 10733523]

Massague J, Wotton D. Transcriptional control by the TGF-beta/Smad signaling system. EMBO J. 2000; 19:1745–1754. [PubMed: 10775259]

Massague J, Blain SW, Lo RS. TGFbeta signaling in growth control, cancer, and heritable disorders. Cell. 2000; 103:295–309. [PubMed: 11057902]

Massague J, Seoane J, Wotton D. Smad transcription factors. Genes Dev. 2005; 19:2783–2810. [PubMed: 16322555]

McLaren A. Primordial germ cells in the mouse. Dev Biol. 2003; 262:1–15. [PubMed: 14512014]

Meersseman G, Verschueren K, Nelles L, Blumenstock C, Kraft H, Wuytens G, Remacle J, Kozak CA, Tylzanowski P, Niehrs C, Huylebroeck D. The C-terminal domain of Mad-like signal transducers is sufficient for biological activity in the *Xenopus* embryo and transcriptional activation. Mech Dev. 1997; 61:127–140. [PubMed: 9076683]

Mishina Y, Suzuki A, Ueno N, Behringer RR. Bmpr encodes a type I bone morphogenetic protein receptor that is essential for gastrulation during mouse embryogenesis. Genes Dev. 1995; 9:3027–3037. [PubMed: 8543149]

Mishina Y, Crombie R, Bradley A, Behringer RR. Multiple roles for activin-like kinase-2 signaling during mouse embryogenesis. Dev Biol. 1999; 213:314–326. [PubMed: 10479450]

Monteiro RM, de Sousa Lopes SM, Korchynskyi O, ten Dijke P, Mummery CL. Spatio-temporal activation of *Smad1* and *Smad5* in vivo: monitoring transcriptional activity of Smad proteins. J Cell Sci. 2004; 117:4653–4663. [PubMed: 15331632]

Nakao A, Afrakhte M, Moren A, Nakayama T, Christian JL, Heuchel R, Itoh S, Kawabata M, Heldin NE, Heldin CH, ten Dijke P. Identification of *Smad7*, a TGFbeta-inducible antagonist of TGF-beta signalling. Nature. 1997; 389:631–635. [PubMed: 9335507]

Oxburgh L, Dudley AT, Godin RE, Koonce CH, Islam A, Anderson DC, Bikoff EK, Robertson EJ. BMP4 substitutes for loss of BMP7 during kidney development. Dev Biol. 2005; 286:637–646. [PubMed: 16154126]

Schier AF. Nodal signaling in vertebrate development. Annu Rev Cell Dev Biol. 2003; 19:589–621. [PubMed: 14570583]

Seoane J, Le HV, Shen L, Anderson SA, Massague J. Integration of Smad and forkhead pathways in the control of neuroepithelial and glioblastoma cell proliferation. Cell. 2004; 117:211–223. [PubMed: 15084259]

Solloway MJ, Robertson EJ. Early embryonic lethality in *Bmp5;Bmp7* double mutant mice suggests functional redundancy within the 60A subgroup. Development. 1999; 126:1753–1768. [PubMed: 10079236]

Solloway MJ, Dudley AT, Bikoff EK, Lyons KM, Hogan BL, Robertson EJ. Mice lacking Bmp6 function. Dev Genet. 1998; 22:321–339. [PubMed: 9664685]

Suzuki A, Chang C, Yingling JM, Wang XF, Hemmati-Brivanlou A. *Smad5* induces ventral fates in *Xenopus* embryo. Dev Biol. 1997; 184:402–405. [PubMed: 9133445]

Tremblay KD, Dunn NR, Robertson EJ. Mouse embryos lacking *Smad1* signals display defects in extra-embryonic tissues and germ cell formation. Development. 2001; 128:3609–3621. [PubMed: 11566864]

Umans L, Vermeire L, Francis A, Chang H, Huylebroeck D, Zwijsen A. Generation of a floxed allele of *Smad5* for cre-mediated conditional knockout in the mouse. Genesis. 2003; 37:5–11. [PubMed: 14502571]

Vincent SD, Dunn NR, Hayashi S, Norris DP, Robertson EJ. Cell fate decisions within the mouse organizer are governed by graded Nodal signals. Genes Dev. 2003; 17:1646–1662. [PubMed: 12842913]

Waldrip WR, Bikoff EK, Hoodless PA, Wrana JL, Robertson EJ. *Smad2* signaling in extraembryonic tissues determines anterior-posterior polarity of the early mouse embryo. Cell. 1998; 92:797–808. [PubMed: 9529255]

Winnier G, Blessing M, Labosky PA, Hogan BL. Bone morphogenetic protein-4 is required for mesoderm formation and patterning in the mouse. Genes Dev. 1995; 9:2105–2116. [PubMed: 7657163]

Yang X, Castilla LH, Xu X, Li C, Gotay J, Weinstein M, Liu PP, Deng CX. Angiogenesis defects and mesenchymal apoptosis in mice lacking SMAD5. Development. 1999; 126:1571–1580. [PubMed: 10079220]

Ying Y, Zhao GQ. Cooperation of endoderm-derived BMP2 and extraembryonic ectoderm-derived BMP4 in primordial germ cell generation in the mouse. Dev Biol. 2001; 232:484–492. [PubMed: 11401407]

Yoshimoto A, Saigou Y, Higashi Y, Kondoh H. Regulation of ocular lens development by Smad-interacting protein 1 involving Foxe3 activation. Development. 2005; 132:4437–4448. [PubMed: 16162653]

Zhang H, Bradley A. Mice deficient for BMP2 are nonviable and have defects in amnion/chorion and cardiac development. Development. 1996; 122:2977–2986. [PubMed: 8898212]

Zhu Y, Richardson JA, Parada LF, Graff JM. *Smad3* mutant mice develop metastatic colorectal cancer. Cell. 1998; 94:703–714. [PubMed: 9753318]

Europe PMC Funders Author Manuscripts

Europe PMC Funders Author Manuscripts

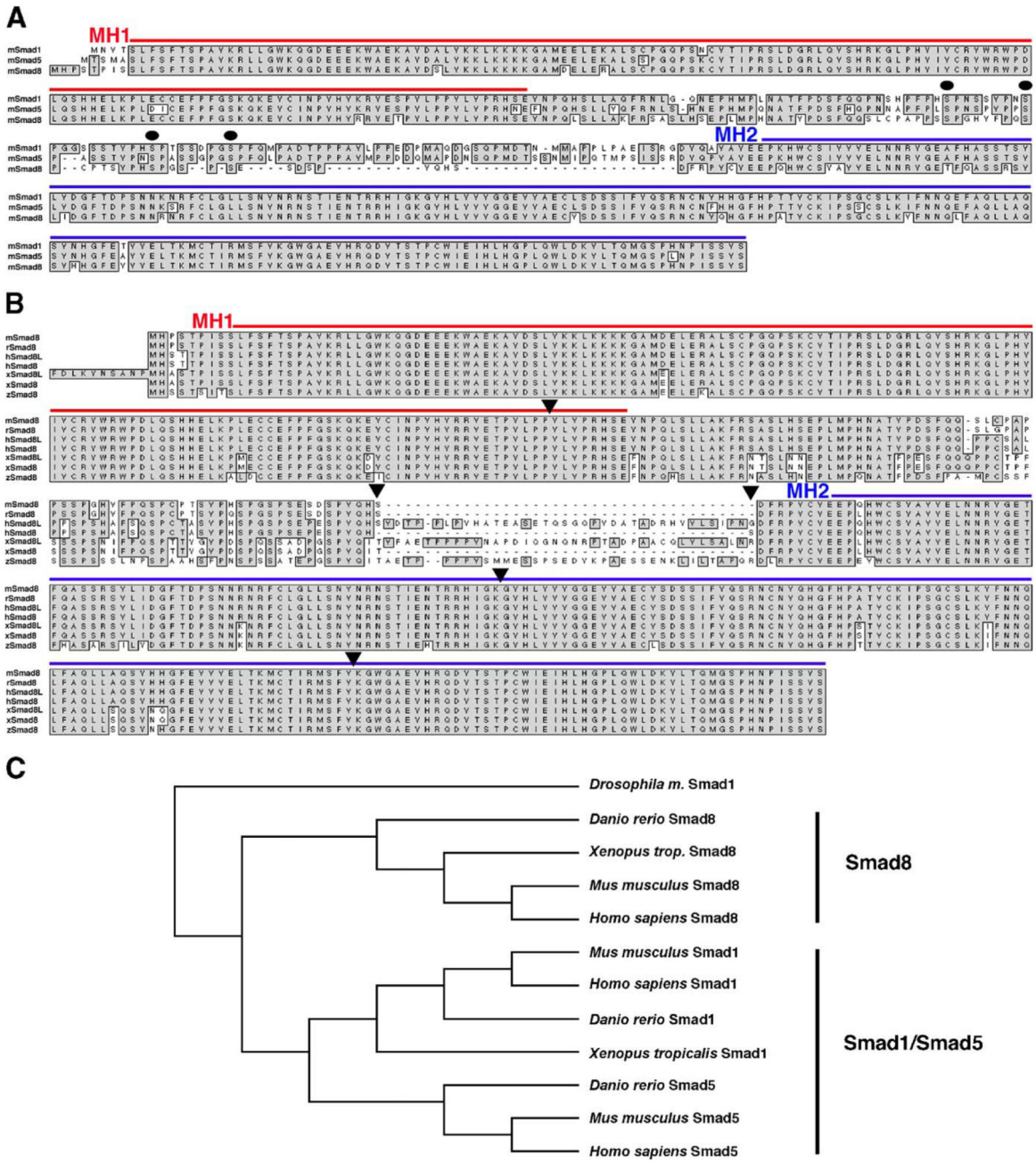

Fig. 1. *Smad1*, *Smad5* and *Smad8* sequence alignments.

(A) Comparison of the *Smad1*, *Smad5* and *Smad8* amino acid sequences in mouse. Boxes show the conserved amino acids. The dots indicate serine residues within Erk-consensus motifs (PXSP). The presumptive boundaries of the MH1and MH2 domains are indicated. (B) The mouse *Smad8* (*mSmad8*) sequence is aligned with those of rat (r), human (h), frog (x) and zebrafish (z). Human and *Xenopus* longer isoforms are indicated as hSmad8L and xSmad8L, respectively. Boxes show conserved amino acids and exon boundaries are denoted by the arrow heads. Sequence alignments were performed using the Macvector software

package (Accelrys.com). (C) A phylogenetic tree of BMP R-Smads shows early branching of *Smad8* from *Smad1* and *5* genes. Fruitfly (*Drosophila melanogaster*), zebrafish (*Danio rerio*), frog (*Xenopus tropicalis*), mouse (*Mus musculus*) and human (*Homo sapiens*). Phylogenetic alignment was generated using Macvector (Accelrys.com).

Europe PMC Funders Author Manuscripts

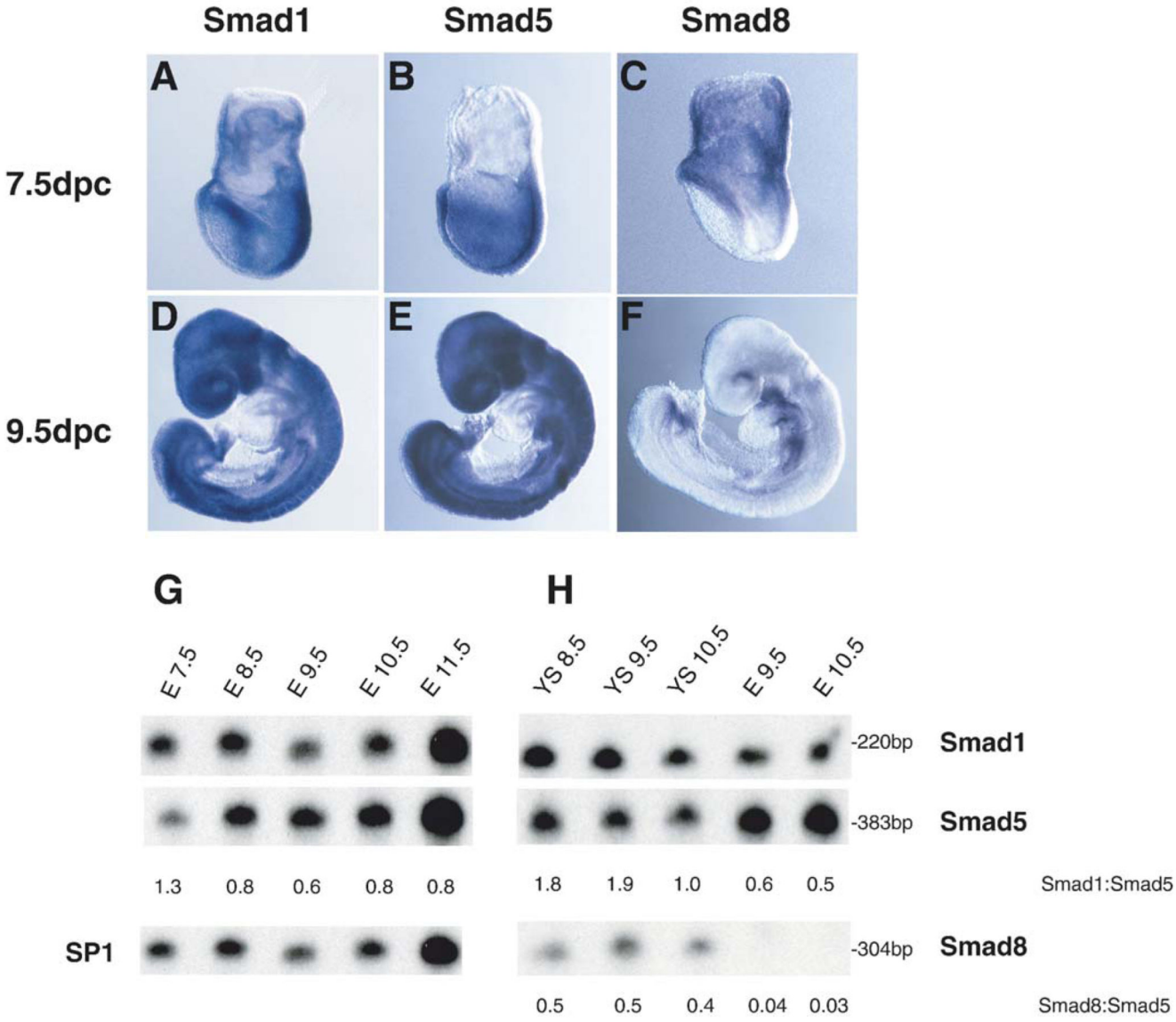

Fig. 2. Partially overlapping *Smad1*, *Smad5* and *Smad8* expression domains in the early mouse embryo.

(A–F) Whole-mount in situ hybridization analysis of *Smad1*, *Smad5* and *Smad8* expression. (A and B) At the early head fold stage (E7.75), *Smad1* and *Smad5* are robustly expressed throughout the extra-embryonic and embryonic regions. (D and E) Similarly at E9.5 both transcripts are widely expressed throughout the embryo proper. (C) In contrast, *Smad8* is exclusively expressed in the extra-embryonic region at E7.75, specifically in the endoderm of the visceral yolk sac (VYS). (F) At E9.5 *Smad8* expression in the embryo is restricted to a subregion of the heart tube and surrounding mesenchyme, the eye and the tail bud. (G and H) Ribonuclease protection assays analyzing *Smad1*, *Smad5* and *Smad8* expression ratios. Total embryonic (E) and yolk sac (YS) RNA at the various stages indicated were tested. The numbers to the right hand side indicate the sizes of the protected fragments. The expression ratios shown as numbers at the bottom of the lanes were calculated by scanning the gels in a

PhosphorImager, measuring the amount of radioactivity in each band and adjusting for the CTP content of the antisense probes. *Smad1* and *Smad5* are co-expressed in the embryo and yolk sac, whereas in contrast *Smad8* transcripts are predominantly localized to the yolk sac. Data shown are representative of 4 independent experiments testing several embryonic and yolk sac total RNA samples.

Europe PMC Funders Author Manuscripts

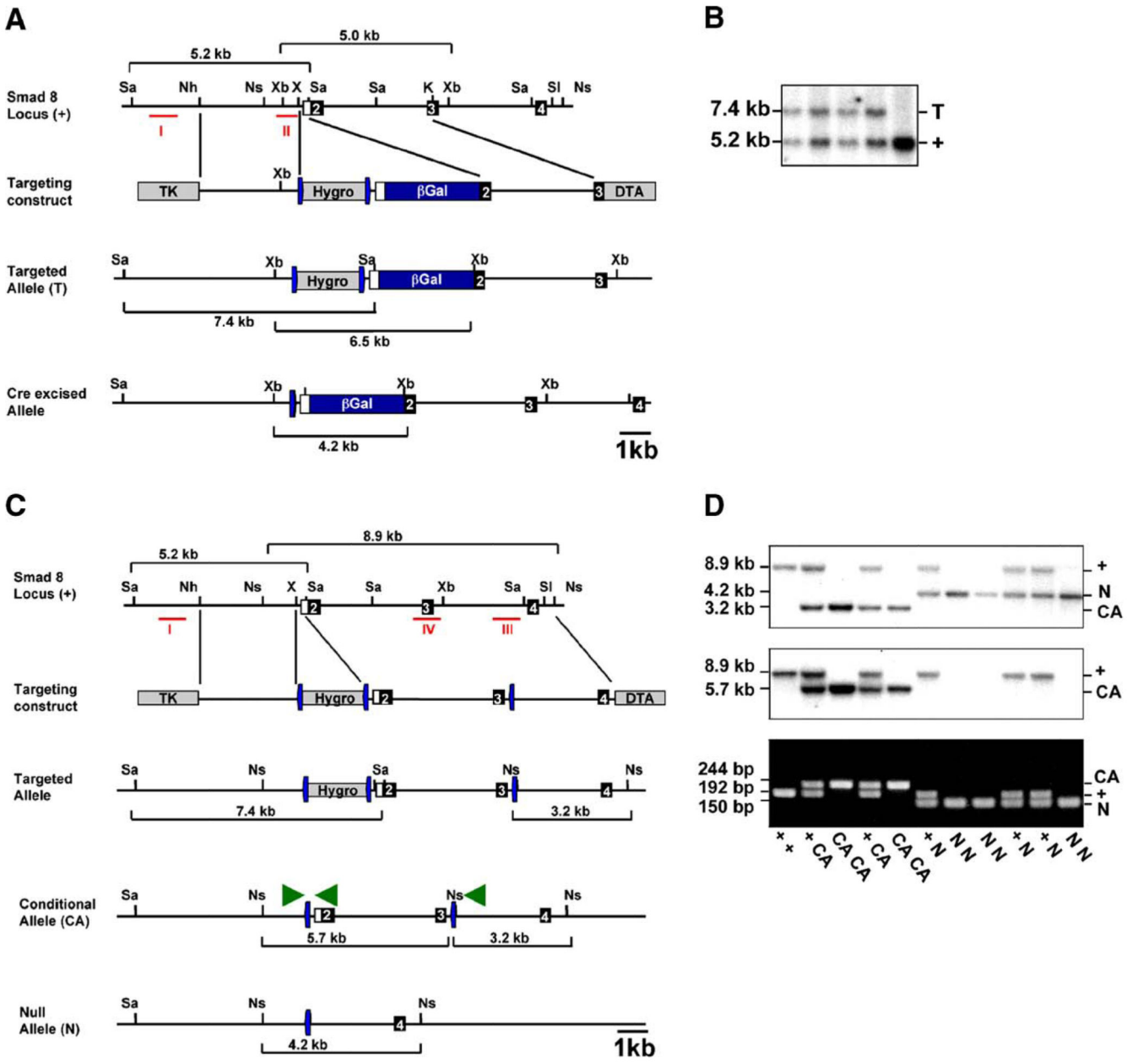

Fig. 3. Generation of *Smad8.LacZ*, conditional and null alleles.

(A) A β-galactosidase-polyA cassette was introduced into the ATG-containing exon 2 of the *Smad8* locus. (B) Hygromycin-resistant ES cell clones were screened by Southern blot analysis of *Sac*I-digested DNA using a 5′ external probe (probe I) that distinguishes 5.2-kb wild-type (+) and 7.4-kb targeted (T) alleles. Correctly targeted clones were subjected to in vitro Cre-mediated excision to remove the loxP (blue arrows)-flanked hygromycin resistance cassette and verified by Southern blot analysis using an internal probe (probe II) on *Xba*I-digested DNA. (C) Targeting strategy for generation of *Smad8* conditional and null alleles. A loxP (blue arrows)-flanked hygromycin resistance cassette was inserted 5′ of exon 2 and a single loxP site placed 3′ of exon 3. Hygromycin-resistant clones were screened by

Southern blot analysis using a 5′ external probe (probe I). Cre-mediated recombination yielded ES cell subclones carrying the conditional (CA) and null (N) alleles. (D) Genotypes of offspring from heterozygous intercross matings. Southern blot analysis of NsiI-digested genomic DNA using a 3′ internal probe (probe III in C) distinguishes 8.9-kb wild-type (+), 3.2-kb conditional (CA) and 4.2-kb null alleles (N). The 3′ internal probe (probe IV in panel C) confirms excision of exons 2 and 3 in homozygous null animals. Confirmatory multiplex PCR genotyping analysis using the indicated primers (green arrowheads in C) distinguishes wt (192 bp), conditional (244 bp) and null allele (150 bp). K, *Kpn*I; Nh, *Nhe*I; Ns, *Nsi*I; Sa, *Sac*I; Sl, *Sal*I; X, *Xho*I; Xb, *Xba*I.

Europe PMC Funders Author Manuscripts

Europe PMC Funders Author Manuscripts

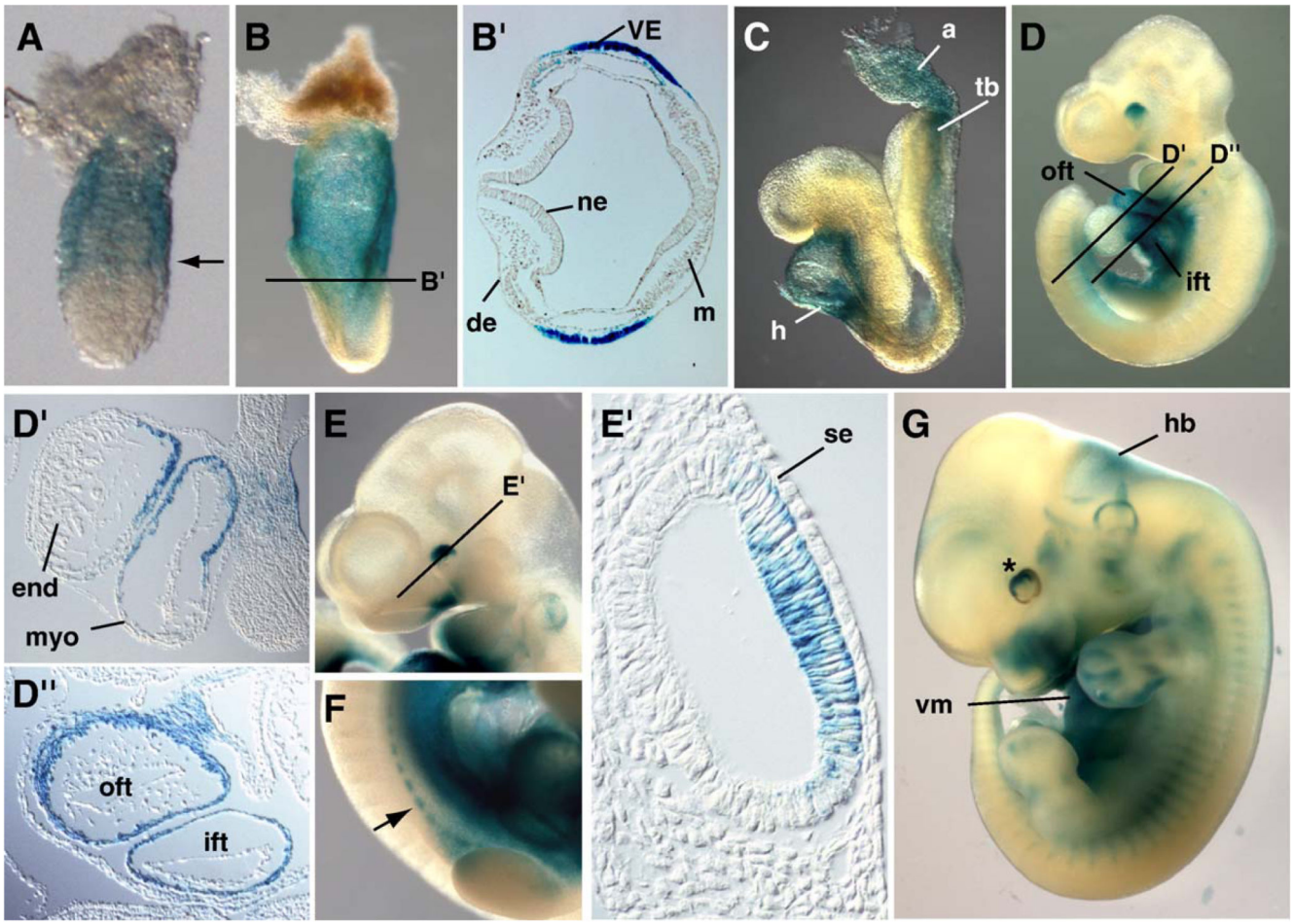

Fig. 4. Highly restricted *Smad8.LacZ* expression during early mouse development.

Whole-mount X-Gal staining of *Smad8.LacZ*/+ embryos at 5.5 dpc (A), 7.5 dpc (B, B′), 8.5 dpc (C), 9.5 dpc (D, D′, D″), 10.5 dpc (E, E′, F) and 12.5 dpc (G). (A, B, B′) *Smad8.LacZ* expression is initially detected in the extra-embryonic visceral endoderm(VE) from day 5.5, but not in the definitive endoderm (de), neuroectoderm (ne) or mesoderm (m) of the embryo proper. (C) *LacZ* expression in the embryo is first detected at 8.5 dpc in the mesenchyme surrounding the forming heart (h) and at lower levels in the tail bud region (tb) and allantois (a). (D, D′, D″) At 9.5 dpc, embryonic expression is strongly seen within the myocardial layer (myo) of the cardiac outflow tract (oft) and inflow tract (ift) but is absent from the forming ventricular regions and endocardium (end). (E, E′) Expression is also initiated within the forming eye and by 10.5 dpc expression is confined to the inner retinal layer of the optic vesicle exclusively in the rostral dorsal half. No expression is seen within the surface ectoderm (se). (F) From E10.5 expression is detectable in the sclerotomal component (arrow) of the somites. (G) At E11.5 X-Gal staining is seen in presumptive areas of chondrogenesis throughout the forming cranial, axial and appendicular skeleton. *LacZ* staining also marks ventral mesenchyme of the thoracic and abdominal regions (vm). Low levels of expression are also seen in the neuroepithelium of the hindbrain (hb) and eye (asterisk).

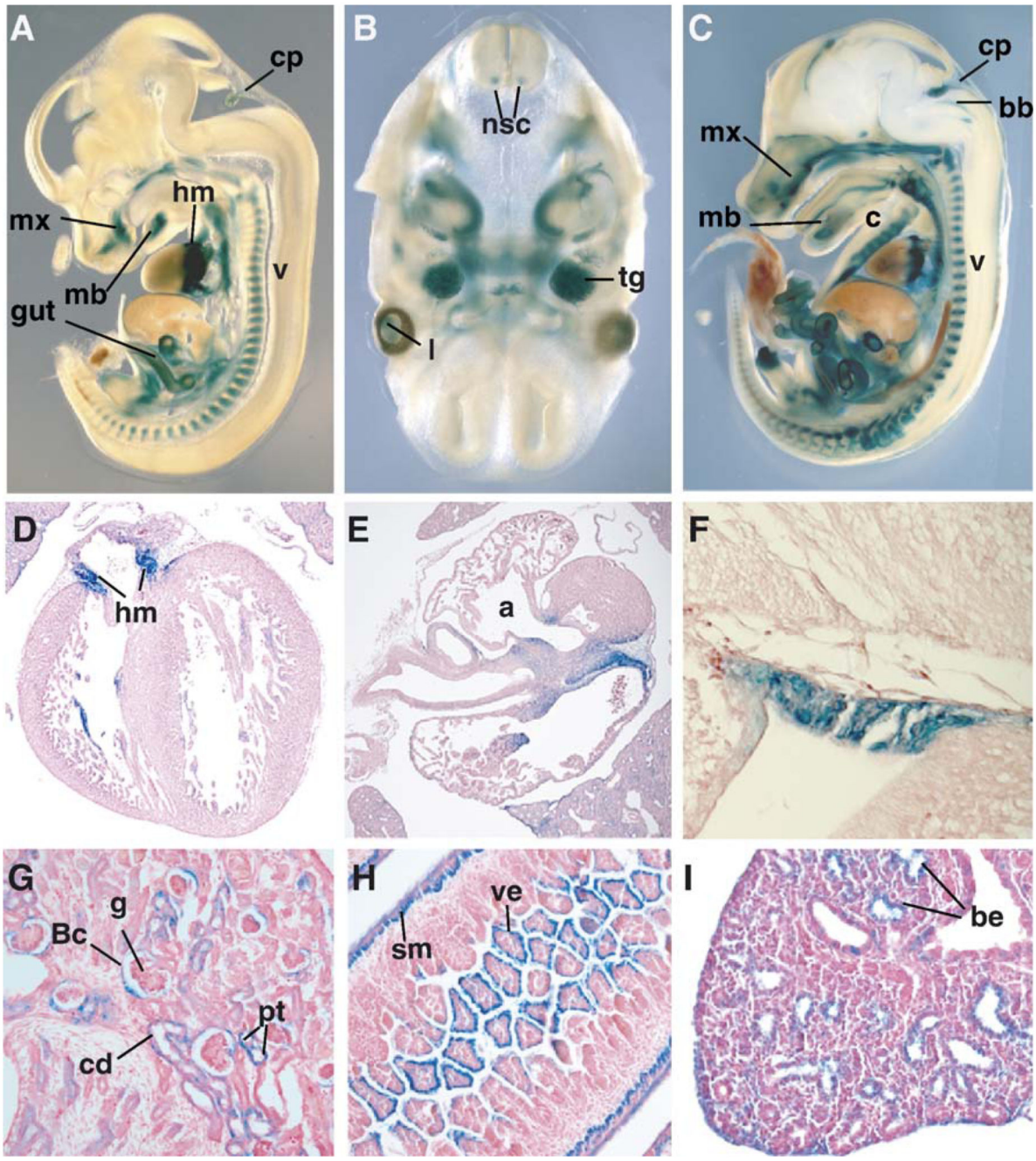

Fig. 5. The *Smad8.LacZ* reporter allele reveals a dynamic pattern of expression during organogenesis.

(A) Sagittal vibratome section of an E14.5 embryo. *LacZ* expression is detected in the choroid plexus (cp), forming vertebra (v), in a band of mesenchyme located in the atrioventricular regions of the developing heart (hm) and in the developing gut. (B) Transverse section of the brain of a 16.5 dpc embryo showing *LacZ* expression in a subset of motorneurons in the anterior spinal cord (nsc), the trigeminal ganglion (tg) and the lens (l). (C) Sagittal vibratome section of an E16.5 embryo. *LacZ*-positive sites include all of the cartilage primordia. In this particular section, cartilage primordia of the vertebrae (v), ribs

(c), basioccipital bone (bb) and forming maxilla (mx) and mandible (mb) are clearly stained. (D and E) Transverse and coronal sections of 16.5 dpc heart showing expression of the *Smad8* reporter allele in the mesenchyme tissue (hm) separating the atria (a) from the ventricles. (F) Close-up of the choroid plexus. (G) Sagittal section of an E16.5 kidney reveals *LacZ* expression in the epithelium of the collecting ducts (cd) and proximal tubules (pt) as well as in the juxtaglomerular apparatus and Bowman's capsule (Bc) of the glomeruli (g). (H) Transverse section of the intestine of a 16.5 dpc embryo. Stained cells correspond to the epithelium layer of the villi (ve). The outer smooth muscle layer (sm) is also positive for *LacZ* expression. (I) At E16.5, within the lung *LacZ* expression is detectable in the epithelial cells of the bronchiole (be).

Europe PMC Funders Author Manuscripts

Europe PMC Funders Author Manuscripts

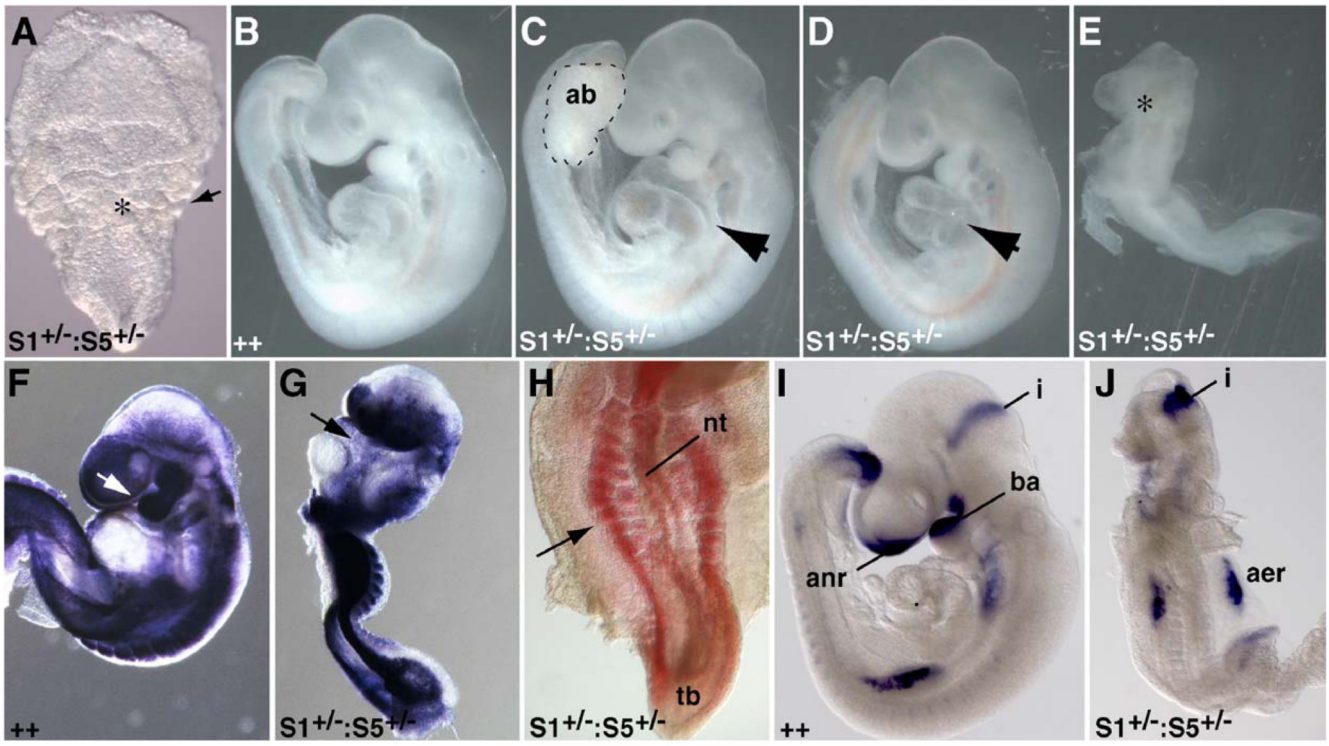

Fig. 6. *Smad1* $^{+/-}$:*Smad5* $^{+/-}$ double heterozygous embryos display pleiotropic tissue abnormalities.

(A) The earliest abnormality seen in a proportion of embryos at E7.5 is ruffling of the visceral yolk sac (asterisk). The arrow marks the boundary between the embryo and extra-embryonic regions. At E9.5, in contrast to wild-type litter mates (B) where the allantois has fused to the chorion, *Smad1* $^{+/-}$:*Smad5* $^{+/-}$ double heterozygotes (C) display an unfused allantoic bud (ab, outlined with dashed line). In this example, the remainder of the embryo is grossly normal including the heart (arrow). (D) Approximately two thirds of mutant embryos show abnormalities in heart morphogenesis including heart looping (arrow in panel D) and patterning defects. (E) Approximately one third of mutant embryos arrest at embryonic turning and show severe defects including lack of anterior neural structures (asterisk). (F, G) In situ hybridization for *Twist* expression in wild-type (F) and mutant embryos (G) shows that severely affected embryos have a paucity of mesoderm and lack branchial arches (arrows in panels F and G). (H) Ventral view of the caudal region of a severely affected embryo shows that the somites are disorganized and fragmented (arrow). (I, J) Analysis of *Fgf8* expression in wild-type (I) and severely affected (J) embryos documents the absence of anterior-most neural tissue whereas the midbrain/hindbrain isthmus (i) is specified. The developing limb buds form but are disorganized. (ab, allantoic bud; aer, apical ectodermal ridge; anr, anterior neural ridge; ba, branchial arch; nt, neural tube; i, isthmus; tb, tail bud).

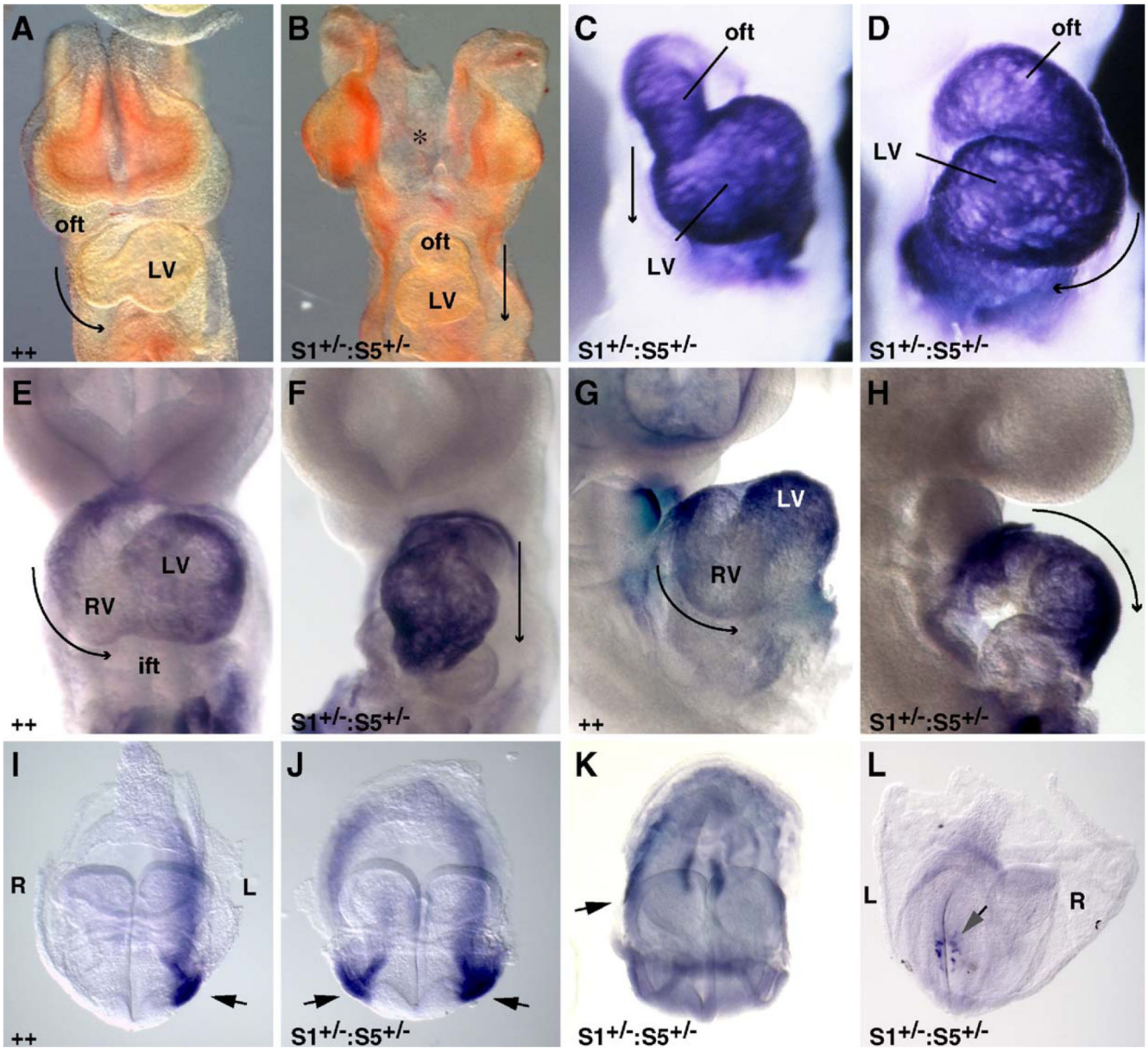

Fig. 7. L/R and heart patterning defects in *Smad1* $^{+/-}$:*Smad5* $^{+/-}$ double heterozygous embryos.

(A, B) Frontal views of E9.5 wild-type and mutant embryos. The arrows indicate the direction of cardiac looping. Normally, the heart tube is looped to the right and the left ventricle (LV) is readily seen. In contrast, in a proportion of *Smad1* $^{+/-}$:*Smad5* $^{+/-}$ mutants, the heart fails to loop and the forming left ventricle remains caudal. The asterisk marks the unfused anterior neural folds in mutants. (C) Staining of hearts with *myosin light chain V* (*MLCV*) highlights the disturbances to heart tube morphogenesis and (D) reversal in the direction of heart looping. (E, G) *eHand* expression in E9.5 wild-type embryos delineates the outer curvature of the left ventricle. Staining is largely absent from the forming right ventricle. (F, H) In *Smad1* $^{+/-}$:*Smad5* $^{+/-}$ embryos, the domain of *eHand* expression has expanded to encompass the length of the heart tube. (I) At E8.5 *Nodal* is normally expressed

in the lateral plate mesoderm on the left side of the axis. *Smad1* $^{+/-}$:*Smad5* $^{+/-}$ embryos show bilateral (J), right-sided (K) *Nodal* expression or in the majority of cases fail to activate asymmetric expression, whereas in the node, *Nodal* is expressed appropriately (L, posterior view) (ift, inflow tract; L, left side of embryo; LV, left ventricle; oft, outflow tract; R, right side of embryo; RV right ventricle).

Europe PMC Funders Author Manuscripts

Europe PMC Funders Author Manuscripts

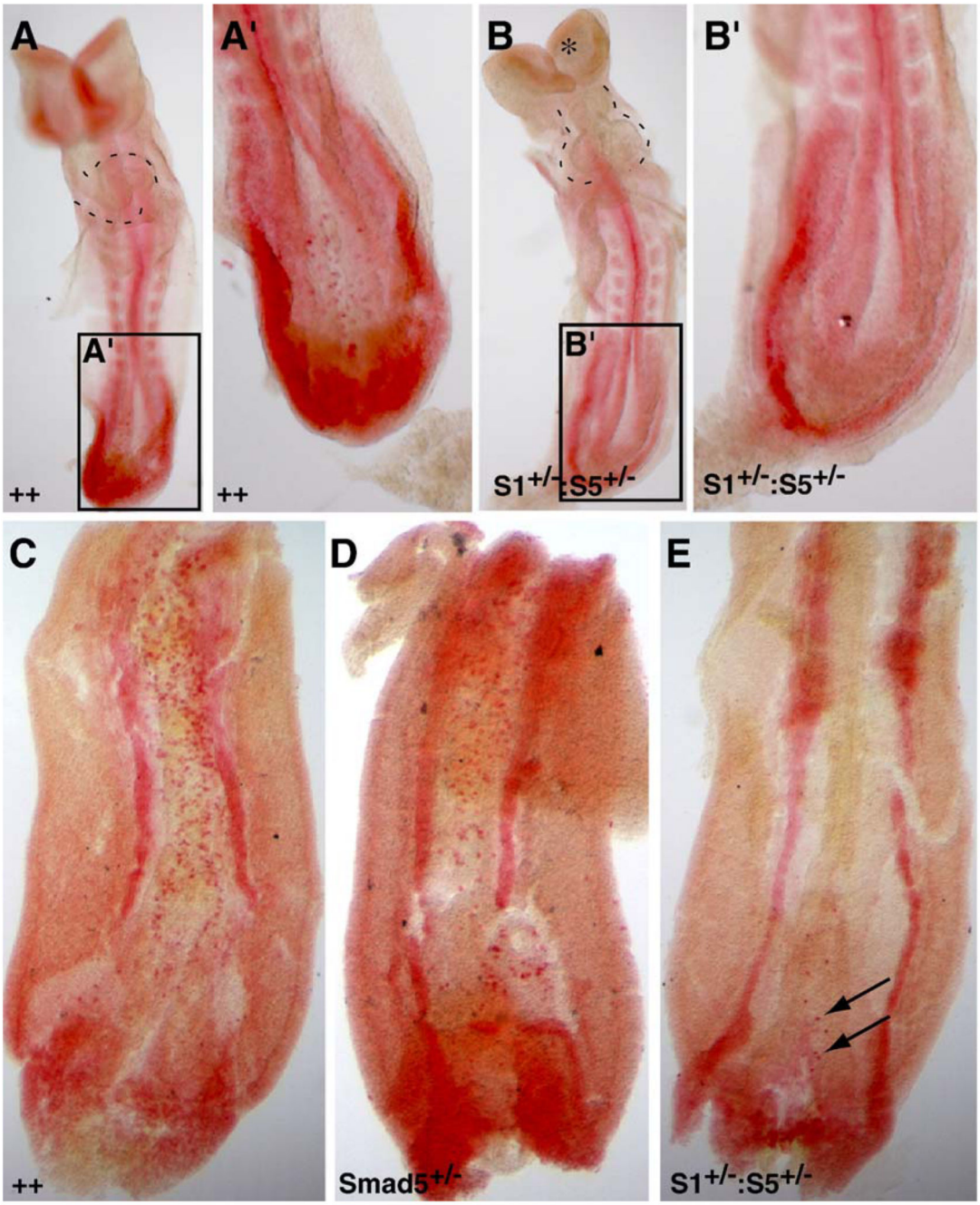

Fig. 8. Dose-dependent *Smad1*/*Smad5* activities are essential for specification of primordial germ cells.

(A, A′, B, B′) Fast red alkaline phosphatase staining of primordial germ cells (PGCs) in E8.5 (A, A′) wild-type and (B, B′) *Smad1* $^{+/-}$:*Smad5*$^{+/-}$ double heterozygous mutant embryos. The mutants display a significant reduction in number of primary germ cells within the hindgut region (compare panel A′ to B′) and additional tissue defects as indicated (heart morphogenesis, dashed line; unfused anterior neural folds, asterisk). (C, D, E) At E9.5, germ cells defects become more pronounced (compare panel C to E, arrows

indicating few detectable PGCs). *Smad5* $^{-/-}$ heterozygous embryos display PGCs at intermediate numbers (D).

Europe PMC Funders Author Manuscripts

Table 1

Genotypes of offspring from *Smad1*, *Smad5* and *Smad8* heterozygous intercrosses

A. *Smad8* $^{+/-}$ × *Smad8* $^{+/-}$

Genotype	*Smad8* $^{+/+}$	*Smad8* $^{+/-}$	*Smad8* $^{-/-}$
No. of animals	45	81	55
Percentage	24.8	44.8	30.3
Expected %	25	50	25

B. *Smad8* $^{+/-}$:*Smad1* $^{+/-}$ × *Smad8* $^{+/-}$:*Smad1* $^{+/-}$

Genotype	*Smad8* $^{+/+}$, *Smad1* $^{+/+}$	*Smad8* $^{+/+}$, *Smad1* $^{+/-}$	*Smad8* $^{+/-}$, *Smad1* $^{+/+}$	*Smad8* $^{+/-}$, *Smad1* $^{+/-}$	*Smad8* $^{-/-}$, *Smad1* $^{+/+}$	*Smad8* $^{-/-}$, *Smad1* $^{+/-}$
No. of animals	17	21	44	39	18	21
Percentage	10.6	13.1	27.5	24.4	11.25	13.1
Expected	12.5	12.5	25	25	12.5	12.5

C. *Smad8* $^{+/-}$:*Smad5* $^{+/-}$ × *Smad8* $^{+/-}$:*Smad5* $^{+/-}$

Genotype	*Smad8* $^{+/+}$, *Smad5* $^{+/+}$	*Smad8* $^{+/+}$, *Smad5* $^{+/-}$	*Smad8* $^{+/-}$, *Smad5* $^{+/+}$	*Smad8* $^{+/-}$, *Smad5* $^{+/-}$	*Smad8* $^{-/-}$, *Smad5* $^{+/+}$	*Smad8* $^{-/-}$, *Smad5* $^{+/-}$
No. of animals	13	17	27	32	14	16
Percentage	10.9	14.3	22.7	26.9	11.8	13.4
Expected	12.5	12.5	25	25	12.5	12.5

D. *Smad8* $^{-/-}$:*Smad5* $^{-/-}$ × *Smad8* $^{-/-}$:*Smad1* $^{+/-}$

Genotype	*Smad8* $^{-/-}$, *Smad5* $^{+/+}$, *Smad1* $^{+/+}$	*Smad8* $^{-/-}$, *Smad5* $^{+/-}$, *Smad1* $^{+/+}$	*Smad8* $^{-/-}$, *Smad5* $^{+/+}$, *Smad1* $^{+/-}$	*Smad8* $^{-/-}$, *Smad5* $^{+/-}$, *Smad1* $^{+/-}$
No. of animals	44	34	43	0
Percentage	35.5	28.1	35.5	0
Expected	25	25	25	25

Europe PMC Funders Author Manuscripts

Table 2

Smad1 $^{+/-}$ ***:Smad5*** $^{+/-}$ **double heterozygous embryos and mutants entirely lacking *Smad1* or *Smad5* share partially overlapping tissue abnormalities**

Defects	Ruffled VYS	Allantois defects	YS vascularization defects	Heart looping defects	L/R axis defects	Turning defects	Branchial arch defects	PGC defects
Genotype								
A. *Smad1* $^{-/-}$, *Smad5* $^{+/+}$	Yes	Yes	NO	ND	ND	NO	NO	Yes
B. *Smad5* $^{-/-}$, *Smad1* $^{+/+}$	NO	Yes	Yes	Yes	Yes	Yes	Yes	Yes
C. *Smad1* $^{+/-}$, *Smad5* $^{+/-}$	Yes	Yes	NO	Yes	Yes	Yes	Yes	Yes

Pleiotropic tissue disturbances were described by (A) Tremblay et al. (2001); (B) Chang et al. (1999); or (C) in this report. ND, not determined.